ABL: Leveraging Millimeter Wave Pulses for Low Latency IoT Networking

Bingwu Fang*, Jonathan Oostvogels*, Xinlei Liu†, Andrey Belogaev†, Sam Michiels*, Danny Hughes*, Jeroen Famaey†
*DistriNet, KU Leuven, Leuven, Belgium
†IDLab, University of Antwerp - imec, Antwerp, Belgium
Email: {bingwu.fang, jonathan.oostvogels, sam.michiels, danny.hughes}@kuleuven.be
Email:{xinlei.liu, andrey.belogaev, jeroen.famaey}@uantwerpen.be

***Abstract*—There is growing demand for low latency and high reliability wireless control of cyber-physical systems. The utilization of millimeter-wave (mm-wave) frequency bands, ranging from 30GHz to 300GHz and offering multi-gigahertz of bandwidth, presents a promising approach to enhance network capacity and transmission speeds, thereby diminishing latency. However, despite mm-wave's potential, achieving these rates in realistic application scenarios is challenging due to poor signal propagation caused by factors such as directional antennas, path loss and occlusion. In response, we propose Asynchronous Burst Link (ABL), an innovative multi-hop mesh network architecture which employs symbol-synchronous transmission of mm-wave pulses. This method mitigates transmission errors by using spatially distributed and closely network synchronised relays to enhance coverage, reduce latency, and improve reliability. Our evaluation of ABL involves a simulated 9-node network with a maximum of 8 hops, utilizing 32-bit packets. The results indicate that latency for the most distant node remains under 1 millisecond, while maintaining 99% reliability. Our findings present evidence for the efficacy of novel mm-wave transceiver architectures in meeting the low latency and robustness demands of network services crucial for critical industrial applications.**

***Index Terms*—Internet of Things, cyber-physical systems, millimeter wave communication, concurrent transmission, low latency communication**

I. Introduction

As a key enabler of the 4th Industrial Revolution or 'Industry 4.0', the Internet of Things (IoT) boosts industrial efficiency through the interconnection of sensors, machines, and devices. In various high-precision domains including robotic actuators, laser cutting systems, spindle control mechanisms, and exact arm positioning technologies, there exists a stringent latency specification at the millisecond scale, coupled with high reliability requirements [1], which is beyond the capability of conventional wireless networks [2].

IoT mesh networking has emerged as a scalable solution for large and/or cluttered environments. However, achieving both high reliability and low latency presents a significant challenge. For example, Bluetooth Mesh latency may be as high as multiple seconds, with double digit rates of packet loss [3]. WirelessHART, SmartMesh-IP and 6TiSCH are designed for real-time process monitoring and control, delivering high reliability with low error rates. However, these approaches likewise fail to address End-to-End (E2E) latency challenges. Wireless networks for Industrial Automation for Process Automation (WIA-PA) exhibit near-zero error rates, but still face latency in the tens of milliseconds [4].

Despite significant advancements, existing protocols for IoT mesh networks primarily adopt store-and-forward strategies, necessitating nodes to fully receive a data frame before forwarding it across a mesh. Such strategies fall short in meeting the growing demands of applications that require both high reliability and low latency concurrently. Exploring alternatives to traditional store-and-forward strategies and collision avoidance protocols is essential to effectively fulfill these demands. Concurrent transmission, for example, allows simultaneous signal transmission by multiple nodes through close synchronisation and thus eliminates the need for routing, significantly reducing latency [5].

Additionally, mm-wave technology, operating within the 30-300GHz spectrum, emerges as a key solution to effectively tackle the growing demand for timely data transmission. With extensive spectral resources, mm-wave enables multi-gigabit-per-second data rates, a vital aspect in contemporary high-speed communication networks [6]. The application of mm-wave technology in the wireless control of insulated gate bipolar transistors (IGBTs) serves as a prime example of its potential, attaining approximately 400 ns ultra-low latency [7]. However, this is for a point-to-point communication model and, given the problematic propagation of mm-wave, this is unsuitable for covering large and complex areas, where mesh networking is typically required.

In response to the necessity of low latency mesh networking, we propose a novel mm-wave mesh network paradigm; Asynchronous Burst Link (ABL). Our main contributions are as summarized as follows:

- We introduce the first *symbol-synchronous* mm-wave radio protocol, a technique heretofore exclusive to Optical Wireless Communication (OWC) [8]. By employing a symbol-synchronous approach, one-hop neighbors selectively and quickly relay signals corresponding to identical bits without feedback loops or channel estimation. This novel integration effectively reduces latency and simplifies meshed system architecture. Additionally, the multi-hop mesh architecture of ABL effectively extends the coverage of mm-wave communications.

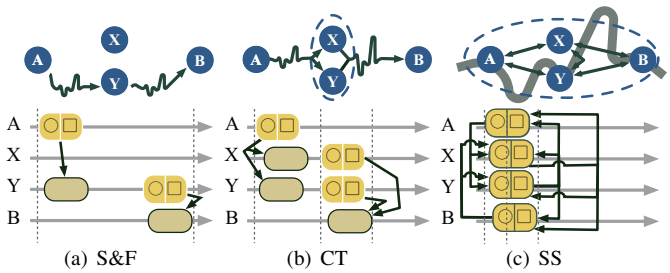

Fig. 1: Transmission methods (a) store-and-forward (S&F), (b) concurrent packet transmission (CT) and (c) symbol synchronous (SS) [8].

- We introduce a novel modulation scheme, *Differential Pulse (DP)* modulation, which ensures reliable network service and addresses errors caused by destructive interference between concurrent signal transmissions, as well as mitigates environmental background noise.

These contributions are simulated using MATLAB R2023b with the Communications Toolbox, and their evaluation demonstrates promising results, including sub-millisecond latency with 99% reliability across a 9-node mesh network featuring a maximum of 8 hops, employing 32-bit packets. The lack of a time-synchronisation requirement between ABL nodes is a perfect fit with recent initiatives in the area of crystal-free radios, such as the Single Chip Micro Mote (SCμM) [9]. Prototype SCμM motes are now available with mm-wave.

This paper is organized as follows: Section II introduces the background including store-and-forward, concurrent transmission and symbol synchronous transmission. Section III details the proposed DP modulation and demodulation scheme, and the design of ABL, Section IV demonstrates and analyzes experimental evaluations, and Section V concludes the work.

II. Background

In this section, we give a brief introduction of store-and-forward technology, followed by a discussion of non-store-and-forward technology, that is, concurrent and symbol synchronous transmission, laying the groundwork for our proposed mechanism.

A. Store-and-Forward

In wireless mesh networks, reliability is challenged by collisions and interference. Techniques such as Carrier Sense Multiple Access (CSMA) and Time Synchronised Channel Hopping (TSCH) mitigate these issues by minimizing collisions and re-transmissions, while store-and-forward routing preserves data integrity and facilitates orderly traffic flow. Together, these strategies synergize to provide reliable network service [5]. However, these approaches achieve reliable networking at the expense of latency.

As depicted in Fig. 1(a), protocols based on store-and-forward require nodes to sequentially receive, check, and forward data. Concretely, node A senses the channel state to prevent collisions and/or schedules data transmissions to node Y based on a routing strategy. Once the packet is fully received, node Y, in turn, assesses the channel state and /or waits for a transmit slot before forwarding the packet according to the routing policy and so on to the subsequent destination. While reliable store-and-forward networking is widely available, the necessity of fully receiving packets, monitoring channel states, checking routing information, and waiting for a transmission slot results in high E2E latency that scales quickly with the number of hops [8].

B. Concurrent Transmission

Concurrent Transmission protocols allow multiple nodes to broadcast packets simultaneously [10], as shown in Fig. 1(b). Thanks to the capture effect and non-destructive interference, nodes are likely to receive at least one of these simultaneous transmitted signals correctly [5].

Glossy, a pioneering concurrent transmission approach, achieves a few milliseconds latency and 99.99% reliability [11]. In Glossy, an initiator starts the broadcast process in a half-duplex way. Once the one-hop neighbors of the initiator have received signal, they re-broadcast in close synchrony. The signal is re-transmitted in a broadcast way until all nodes receive it successfully.

Recent works have demonstrated the versatility of concurrent transmission mechanisms, extending beyond their initial application in IEEE 802.15.4 [11]. This approach is now effectively implemented in various technologies, including Ultra-WideBand (UWB) [12], Bluetooth Low Energy (BLE) [13], and Long Range (LoRa) [14]. These advancements underscore the adaptability of concurrent transmissions across different physical layers, establishing a solid groundwork for their integration into mm-wave technology.

C. Symbol Synchronous Transmission

Prior research on concurrent transmissions has primarily focused on packet-wise operations, which naturally results in packet-scale latency [11], [13], [14], quantified on at least millisecond level. Zero-Wire [8], however, introduces a novel approach by implementing a symbol-synchronous bus network protocol that operates at the level of the smallest unit of transmission (i.e. the symbol), allowing for dramatically lower multi-hop latency.

This mechanism allows relay nodes to immediately forward symbols upon detection, without coordinating with others, and without making transmission decisions based on the contents of the signal, thus achieving sub-millisecond E2E latency. In symbol synchronous transmission, nodes relay incoming symbols with a relay time offset D_{offset}, such that the time difference D_{jitter} between the moment the first instance of a symbol originally transmitted by the initiator is detected ($T_{firstArrival}$) and the detection of the last instance ($T_{latestArrival}$), due to different relay paths, is smaller than the symbol duration, as formalised below.

$$D_{jitter} = T_{latestArrival} - T_{firstArrival} \quad (1)$$

$$D_{jitter} < D_{symbol} \quad (2)$$

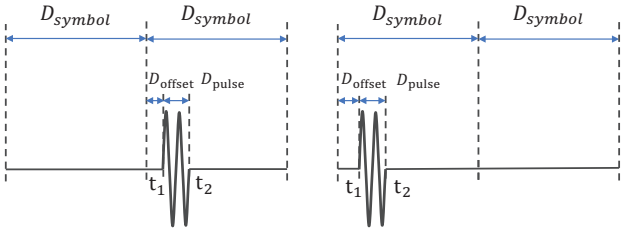

(a) Bit 0: Amplitude DP (b) Bit 1: Amplitude DP

Fig. 2: DP Modulation scheme for 0/1 binary information representation.

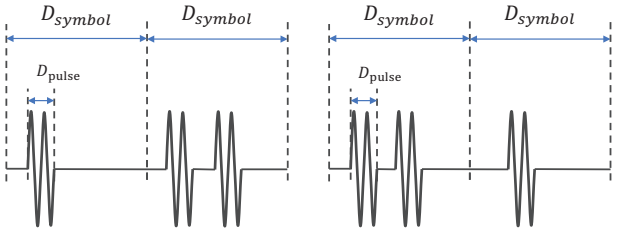

(a) Bit 0: Existing times DP (b) Bit 1: Existing times DP

Fig. 3: DP Demodulation scheme for 0/1 binary information representation.

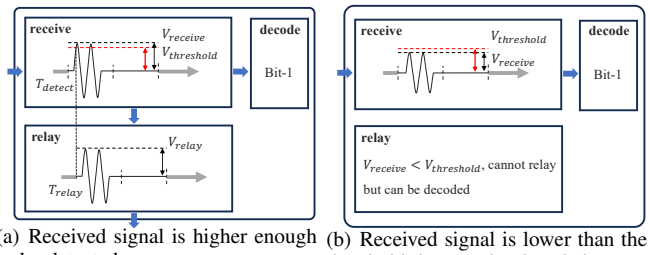

(a) Received signal is higher enough to be detected (b) Received signal is lower than the threshold, but can be decoded

Fig. 4: Signal receiving, detection, relaying, and decoding

Under condition (2), signals are forwarded only if the initial reception and subsequent relay to the same node occur within a period less than the symbol duration. This ensures effective symbol propagation across one-hop neighbors, effectively preventing a cycle of re-relaying identical symbols by the same nodes.

III. System Design of ABL

This section describes the design of ABL starting from the proposed Differential Pulse (DP) Modulation scheme in Section III-A, then followed by the comprehensive ABL protocol in Section III-B. Finally, we describe how the system can be integrated with conventional mm-wave hardware in Section III-C.

A. Differential Pulse Modulation

In Zero-Wire [8], optical signals are propagated symbol-synchronously, with simultaneous transmission of identical symbols by one-hop neighbors. This system employs On-Off Keying (OOK) for data encoding, modulating ambient light intensity levels. Unlike the optical media of the original Zero-Wire systems, radio-based systems require techniques to address destructive interference which occurs due to the use of *coherent* transmitters in conventional radios. To mitigate these problems, it is essential to develop an efficient modulation and demodulation scheme that circumvents destructive interference through redundancy in time and frequency space.

Inspired by Time Spread On-Off Keying (TS-OOK) modulation with pulse signals in Terahertz communication [15], we propose the Differential Pulse (DP) modulation scheme. The details are as follows.

Modulation: In the DP modulation scheme, binary information is encoded through the variation in maximum amplitude as depicted in Fig. 2. The source of the signal, or *initiator*, encodes binary information by toggling a sine wave signal generator On and Off at predetermined intervals. Concretely, with the proposed DP scheme, bit-1 is encoded by a "pulse exists" symbol followed by a "silence" symbol, and vice versa for a bit-0, as demonstrated in Fig. 2(a) and Fig. 2(b). Note that in real systems, the symbol duration may be many times longer than the pulse duration, which has here been tailored for visual clarity. The corresponding representation of 0/1 binary information is as follows:

$$S^0 = \begin{cases} A \cdot \sin\left[2\pi \cdot f_c \cdot (t - D_{offset}) + \phi\right] \\ \text{when } 0 \le t_1 < t < t_2 \le D_{symbol}, \\ 0 \\ \text{when } \{t | t \in [0, 2 \cdot D_{symbol}] \, \Lambda t \notin [t_1, t_2]\} \end{cases} \tag{3}$$

$$S^1 = \begin{cases} A \cdot \sin\left[2\pi \cdot f_c \cdot t + \phi\right] \\ \text{when } D_{symbol} \le t_1 < t < t_2 \le 2 \cdot D_{symbol}, \\ 0 \\ \text{when } \{t | t \in [0, 2 \cdot D_{symbol}] \, \Lambda t \notin [t_1, t_2]\} \end{cases} \tag{4}$$

where A is the amplitude of the pulse and f_c is the frequency of the sine wave pulse. The timing offset, denoted as D_{offset}, arises due to hardware imperfections, ϕ is the phase shift of the signal, $\phi \in [0, 2\pi]$. D_{symbol} is the duration of symbol. The duration of a pulse is,

$$D_{pulse} = t_2 - t_1 \tag{5}$$

It is much smaller than the symbol duration, i.e.,

$$D_{pulse} \ll D_{symbol} \tag{6}$$

The relationship between D_{pulse} and D_{symbol} can be simply illustrated as,

$$D_{symbol} = \beta \cdot D_{pulse} \tag{7}$$

where $\beta > 0$. In our proposed DP scheme, 1-bit data is encoded using a pair of consecutive symbols, thereby, the duration for 1-bit binary information is

$$D_{bit} = 2 * D_{symbol} \tag{8}$$

Demodulation: As depicted in Fig. 2(a), a signal is decoded as bit-0 if the amplitude of the pulse signal in the first symbol, $\max\left(A_{pulse}^{1st}\right)$, is less than in the subsequent symbol,

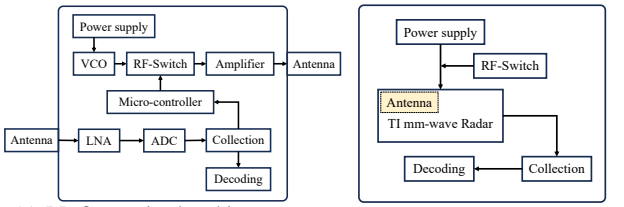

(a) LL fine-grained architecture (b) HL modular implementation

Fig. 5: ABL system architecture

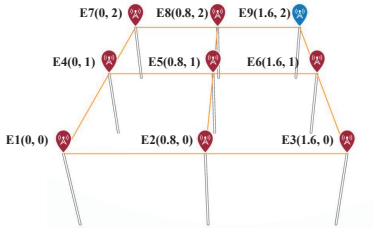

Fig. 6: Network topology

$\max\left(A^{2nd}_{pulse}\right)$ and vice versa for bit-1, as shown in Fig. 2(b). Moreover, as shown in Fig. 3(a), a signal is decoded as bit-0 if the maximum time of pulse signal exist in the first symbol $\max\left(T^{1st}_{pulse}\right)$ is shorter than that in the following symbol $\left(T^{2nd}_{pulse}\right)$, and vice versa for bit-1, as shown in Fig. 3(b). The differential factor is defined as(11)(12). If $F_a > F_t$, the demodulation scheme base on the amplitude difference, otherwise base on the maximum time difference. Concretely:

$$bit-0 = \begin{cases} \max\left(A^{1st}_{pulse}\right) < \max\left(A^{2nd}_{pulse}\right) \\ \max\left(T^{1st}_{pulse}\right) < \max\left(T^{2nd}_{pulse}\right) \end{cases} \quad (9)$$

$$bit-1 = \begin{cases} \max\left(A^{1st}_{pulse}\right) > \max\left(A^{2nd}_{pulse}\right) \\ \max\left(T^{1st}_{pulse}\right) > \max\left(T^{2nd}_{pulse}\right) \end{cases} \quad (10)$$

$$F_a = abs(A^{1st}_{pulse} - A^{2nd}_{pulse})/min(A^{1st}_{pulse}, A^{2nd}_{pulse}) \quad (11)$$

$$F_t = abs(T^{1st}_{pulse} - T^{2nd}_{pulse})/min(T^{1st}_{pulse}, T^{2nd}_{pulse}) \quad (12)$$

B. ABL Protocol

In our ABL system, nodes continuously sample and detect the amplitude of incoming signals to decide whether to re-transmit. If the amplitude is higher than a predefined threshold, a node re-transmits the incoming pulse with a slight time offset. If the amplitude of signal falls below the predefined threshold, and thus should not be relayed, nodes still attempt to decode the signal. The corresponding procedure is illustrated in Fig. 4.

As shown in Fig. 4, a single node includes three main functions, receiving, relaying base on the signal detection, and decoding according to our proposed signal decoding method. We denote $V_{receive}$ as the amplitude of the received signal, and $V_{threshold}$ as the system configured signal detection threshold, it can be configured adaptively based upon the noise-floor. As shown in Fig. 4(a), if the received signal is higher than $V_{threshold}$, a node starts to relay signal with the amplitude of V_{relay} at detection time T_{detect}. If amplitude of the received signal is not high enough to be detected, but not been fully overwhelmed by the noise, nodes can still decode the signal and get the transmitted data in time, as depicted in Fig. 4(b).

C. ABL architecture

A potential low-level (LL) fine-grained system architecture for ABL is shown in Fig. 5(a). On the transmitter side, a Voltage-Controlled Oscillator (VCO), such as 840UF-29/3830 [16], is employed to generate the 60GHz mm-wave signal. The RF-Switch is controlled by a Micro-controller, facilitating the creation of pulse signals as well as the configuration of pulse duration. These signals are subsequently amplified and transmitted via an antenna. Conversely, on the receiver side, incoming signals captured by the antenna are initially amplified by a Low-Noise Amplifier (LNA). The amplified signals are then digitized by an Analog-to-Digital Converter (ADC), followed by signal processing to decide whether to retransmit.

The ABL system can also be implemented with existing commercial off-the-shelf (COTS) hardware products on top of a higher-level (HL) modulation methods, such as with TI mm-wave radars [17]. Concretely, the corresponding potential hardware architecture is shown in Fig 5(b).

IV. Evaluation

The proposed mechanisms are simulated in Matlab on a 8-core 2.3GHz machine with an 32-GB RAM. In this section, we experimentally analyse latency, reliability and robustness in the presence of blockages.

A. Simulation Set-up

To ensure that our simulation stays close to achievable results, we parameterise our simulation to match current technological standards and hardware platforms. Simulation parameters are configured as shown in Table I and explained in the following text.

TABLE I: Network configuration

Parameter	Value	Note
P_t	20 dBm	Transmission power
f_c	60 GHz	Carrier frequency
f_s	25 MHz	Sampling frequency
D_{pulse}	200 ns	Pulse duration
D_{symbol}	1 μs	Symbol duration
L_{packet}	32 bit	Packet length

In our simulation, we implement a Ray-Tracing propagation model, integrating additive white Gaussian noise. Our focus is solely on Line-of-Sight communication, assuming an environment free of blockages. As shown in Fig. 6, our setup includes 9 nodes, with E1(0,0) designated as the initiator of transmission. Nodes communicate only with their immediate one-hop neighbors due to signal strength limitations. For instance, as shown in Fig. 6, the yellow lines between E1, and

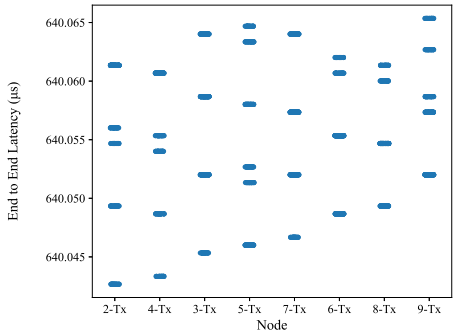

Fig. 7: E2E latency for nodes, with $f_c = 60$GHz, $f_s = 25$MHz, $SNR = 25$dB, $\beta = 50$

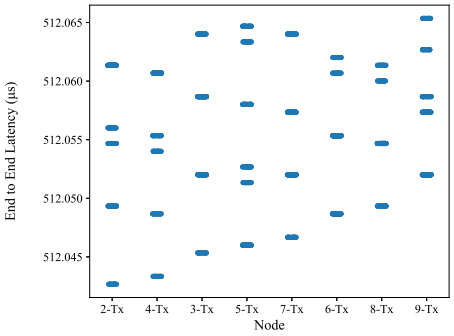

Fig. 9: End to End latency for nodes, with $f_c = 60$GHz, $f_s = 25$MHz, $SNR = 25$dB, $\beta = 40$

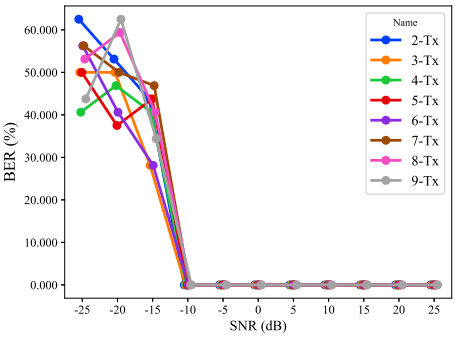

Fig. 8: Bit Error Rate for nodes with $f_c = 60$GHz, $f_s = 25$MHz, $SNR \in [-25, 25]$dB, $\beta = 50$

E2, E4 indicate that E1 communicates with E2 and E4, but not with E5, E3, or E7. When direct communication between the initiator and destination fails, symbols follow a multi-hop route of between 2 and 8 hops.

The carrier frequency f_c is set to 60 GHz, consistent with the specifications delineated in IEEE 802.11ad and IEEE 802.11ay. Given that signal reconstruction is not an objective of our research, strict compliance with the Nyquist–Shannon sampling theorem is deemed non-essential. Consequently, we adopted a sampling frequency f_s of 25 MHz, as specified in the TI sensor IWR6843 [17]. To ensure a sufficient number of sampled points with each pulse duration, we configured D_{pulse} as 200 nanoseconds. Equation (5) demonstrates our approach to achieving a relatively short pulse duration by setting $D_{symbol} = 50 \cdot D_{pulse}$, which for a 1-bit signal means that $D_{bit} = 100 \cdot D_{pulse}$. Finally, the transmission power for each node is modelled on the output capabilities of the widely used HMC 1144 power amplifier [18]. This configuration strikes a balance between technical feasibility and the practical constraints of contemporary hardware, facilitating a robust analysis within the stipulated parameters.

B. Results and Discussion

Latency: Figure 7 illustrates the packet-level E2E latency, which is the time for 32-bit length packet sent from initiator experienced by each node within the network for various path lengths. Due to the concurrent transmission of signals and the absence of routing, packets may follow variable paths, resulting in fluctuating E2E latency. With our current network configuration, when packets of 32 bits traverse a maximum of 8 hops, the observed latency remains below 640μs. The variability in E2E latency for each network node arises primarily from uncertainties in sampling due to phase shifting, time to get to constructive superposition, and the existence of multiple bit transmission paths. As can be seen from Figure 7, latency is rather insensitive to network diameter, increasing slowly with hop count.

Reliability: Figure 8 illustrates the Bit-Error-Rate (BER) for all nodes across varying Signal-to-Noise Ratios (SNR) with the consistent configuration for the E2E latency evaluation as shown in Fig 7. In the evaluation of the DP modulation scheme, a compelling performance profile emerges, particularly in positive SNR environments. The scheme exhibits outstanding efficiency, with the BER nearing zero at SNR levels of -10dB and above. This exceptional performance in favorable SNR conditions demonstrates the scheme's superior noise resilience and reliability, underscoring its suitability for common operational environments where positive SNR is prevalent. While there is a notable decrease in performance below the -10dB, the primary focus remains on the scheme's impressive capabilities in the typical and more frequently encountered positive SNR scenarios. This strength in standard operational contexts highlights the scheme's practical applicability and potential for robust, reliable network communication.

Symbol duration effect: The system's latency performance is influenced in part by its data rate. In our proposed DP data encoding method, the data rate is

$$Rate_{data} = \frac{1}{2 \cdot D_{symbol}} \tag{13}$$

Thus, the data rate can be changed by the configuration of D_{symbol}. For a given D_{pulse}, we make $D_{symbol} = 40 \cdot D_{pulse}$. The results presented in Fig. 9 illustrate a decrease in symbol duration, leading to a corresponding reduction in bit duration. This change notably increases the data rate. Thereby, E2E latency is reduced, as compared to the values depicted in Fig. 7.

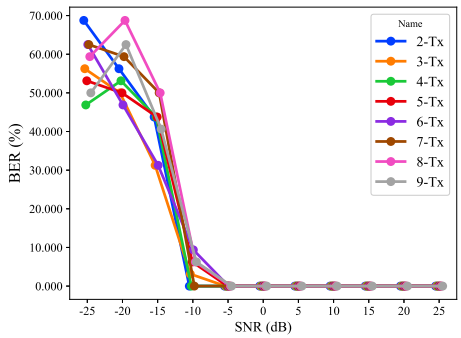

Fig. 10: Bit Error Rate for nodes with $f_c = 60$GHz, $f_s = 25$MHz, $SNR \in [-25, 25]$dB, $\beta = 40$

However, for a given pulse duration, the decrease of the symbol duration also affects reliability. As shown in Fig. 10, the BER performance gets worse with low SNR configurations, because the increase of the proportion of pulse to symbol duration for 1-bit signals increase the probability of destructive interference, which directly affects the reliability of the proposed ABL system.

V. Conclusions

In this work, we introduced ABL, an innovative protocol for IoT mesh networks. ABL is the first radio frequency approach to symbol synchronous communication and includes a novel differential pulse modulation scheme. We evaluate the latency and reliability performance in a 9-node network with a maximum of 8 hops to transmit 32-bit packets. We conducted simulations at a sampling frequency of 25 MHz, revealing that the latency for all nodes could be reduced to less than 650μs. Our Differential Pulse (DP) modulation scheme ensures a system reliability of 99% even at a Signal-to-Noise Ratio (SNR) as low as -10 dB. The numerical results substantiate that our proposed ABL presents an effective strategy for achieving low latency and high reliability, while enhancing mm-wave communication coverage via a spatially redundant multi-hop mesh network architecture. This research thus provides a potential solution for the critical design challenge of mm-wave transceivers, fulfilling the stringent low latency and robustness requirements essential for critical industrial network applications. Our future research will focus on an in-depth analysis of latency performance in comparison to alternative signal processing methodologies, aiming to devise strategies that simultaneously improve data rate and throughput while maintaining robust, low latency network services. We will also focus on realizing a practical implementation of our approach on a crystal-free mm-wave transceiver such as SCuMM from UC Berkeley.

Acknowledgment

This document is issued within the frame and for the purpose of the OpenSwarm project. This project has received funding from the European Union's Horizon Europe Framework under Grant 101093046. Additional support is provided by the FWO as part of the LOCUSTS project (G019722N), J. Oostvogels' fellowship (11H7923N) and the research fund, KU Leuven.

References

[1] K. Montgomery, R. Candell, Y. Liu, and M. Hany, *Wireless user requirements for the factory workcell*. Department of Commerce, National Institute of Standards and Technology, 2020.

[2] M. Vaezi, A. Azari, S. R. Khosravirad, M. Shirvanimoghaddam, M. M. Azari, D. Chasaki, and P. Popovski, "Cellular, wide-area, and non-terrestrial IoT: A survey on 5G advances and the road toward 6G," *IEEE Communications Surveys & Tutorials*, vol. 24, no. 2, pp. 1117–1174, 2022.

[3] R. Rondón, A. Mahmood, S. Grimaldi, and M. Gidlund, "Understanding the Performance of Bluetooth Mesh: Reliability, Delay, and Scalability Analysis," *IEEE Internet of things journal*, vol. 7, no. 3, pp. 2089–2101, 2019.

[4] "Industrial Networks–Wireless Communication Network and Communication Profiles–WIA-PA," International Electrotechnical Commission, IEC Standard PAS 62601, 2015, available: https://webstore.iec.ch/publication/23902.

[5] M. Baddeley, C. A. Boano, A. Escobar-Molero, Y. Liu, X. Ma, V. Marot, U. Raza, K. Römer, M. Schuß, and A. Stanoev, "Understanding Concurrent Transmissions: The Impact of Carrier Frequency Offset and RF Interference on Physical Layer Performance," *ACM Transactions on Sensor Networks*, 2023.

[6] T. S. Rappaport, S. Sun, R. Mayzus, H. Zhao, Y. Azar, K. Wang, G. N. Wong, J. K. Schulz, M. Samimi, and F. Gutierrez, "Millimeter wave mobile communications for 5G cellular: It will work!" *IEEE access*, vol. 1, pp. 335–349, 2013.

[7] K. Yamamoto, F. Ichihara, K. Hasegawa, M. Tukuda, and I. Omura, "60 GHz wireless signal transmitting gate driver for IGBT," in *2015 IEEE 27th International Symposium on Power Semiconductor Devices & IC's (ISPSD)*. IEEE, 2015, pp. 133–136.

[8] J. Oostvogels, F. Yang, S. Michiels, and D. Hughes, "Zero-wire: a deterministic and low-latency wireless bus through symbol-synchronous transmission of optical signals," in *Proceedings of the 18th Conference on Embedded Networked Sensor Systems*, 2020, pp. 164–178.

[9] T. Watteyne, "Crystal-free architectures for smart dust and the industrial IoT," in *2020 7th International Conference on Internet of Things: Systems, Management and Security*. IEEE, 2020, pp. 1–1.

[10] M. Zimmerling, L. Mottola, and S. Santini, "Synchronous transmissions in low-power wireless: A survey of communication protocols and network services," *ACM Computing Surveys (CSUR)*, vol. 53, no. 6, pp. 1–39, 2020.

[11] F. Ferrari, M. Zimmerling, L. Thiele, and O. Saukh, "Efficient network flooding and time synchronization with glossy," in *Proceedings of the 10th ACM/IEEE International Conference on Information Processing in Sensor Networks*. IEEE, 2011, pp. 73–84.

[12] D. Lobba, M. Trobinger, D. Vecchia, T. Istomin, G. P. Picco *et al.*, "Concurrent Transmissions for Multi-hop Communication on Ultra-wideband Radios." in *EWSN*, 2020, pp. 132–143.

[13] B. A. Nahas, A. Escobar-Molero, J. Klaue, S. Duquennoy, and O. Landsiedel, "BlueFlood: Concurrent transmissions for multi-hop Bluetooth 5—Modeling and evaluation," *ACM Transactions on Internet of Things*, vol. 2, no. 4, pp. 1–30, 2021.

[14] X. Xia, N. Hou, Y. Zheng, and T. Gu, "Pcube: scaling lora concurrent transmissions with reception diversities," *ACM Transactions on Sensor Networks*, vol. 18, no. 4, pp. 1–25, 2023.

[15] J. M. Jornet and I. F. Akyildiz, "Femtosecond-long pulse-based modulation for terahertz band communication in nanonetworks," *IEEE Transactions on Communications*, vol. 62, no. 5, pp. 1742–1754, 2014.

[16] Mi Wave, "840EF-17/387, E-band, WR-12, 17 dBm Output Power, 60 GHz-90 GHz Wide Band Voltage Controlled Sources (VCO)," [Online]. Available: https://www.miwv.com/voltage-controlled-oscillators-wide-band-sources-vco-e-band-60ghz-to-90ghz/, 2007.

[17] Texas Instruments, "IWR6843 Single-Chip 60-GHz to 64-GHz mmWave Sensor Data Sheet," 2023, [Online]. Available: http://www.ti.com/lit/ds/symlink/iwr6843.pdf.

[18] Analog Devices, "HMC1144-DIE 35 GHz to 70 GHz, GaAs, pHEMT, MMIC, Medium Power Amplifier," [Online]. Available: https://www.analog.com/media/en/technical-documentation/data-sheets/hmc1144.pdf, 2015.